ELSEVIER

Journal of Atmospheric and Solar-Terrestrial Physics 66 (2004) 1295–1309

Journal of ATMOSPHERIC AND SOLAR-TERRESTRIAL PHYSICS

www.elsevier.com/locate/jastp

Stream structure and coronal sources of the solar wind during the May 12th, 1997 CME

C.N. Arge[a,*], J.G. Luhmann[b], D. Odstrcil[c], C.J. Schrijver[d], Y. Li[b]

[a]*AFRL/VSBXS, Hanscom AFB, MA 01731-3010, USA*
[b]*Space Sciences Laboratory, University of California, Berkeley, CA 94720, USA*
[c]*University of Colorado CIRES and NOAA Space Environment Center, Boulder, CO 80305, USA*
[d]*Lockheed Martin Advanced Technology Center, Department L9-41, Palo Alto, CA 94304, USA*

Received 9 February 2004; received in revised form 15 March 2004; accepted 29 March 2004

Abstract

We report on our efforts to model the ambient solar wind out to 1 AU around the time of the May 12, 1997 halo coronal mass ejection (CME) and to identify its coronal source regions. We use the simple physics and empirical based Wang–Sheeley–Arge (WSA) model driven by two different sets of updated photospheric field synoptic maps to accomplish this: daily updated maps from Mount Wilson Solar Observatory and updated SOHO/MDI maps constructed with the Schrijver et al. flux transport data assimilation algorithm. The results generated by the WSA model are then compared with the WIND satellite observations near Earth, as well as with each other. We find that the model describes the observed ambient solar wind stream structure around the time of the May 12, 1997 CME generally well, except for the ejecta itself. Our results suggest that the source of the high-speed stream that followed the CME is a coronal hole extension located south of the Sun's equator. We conclude that the northern active region associated with the May 12th CME did not play a role in the formation of the small southern coronal hole extension that produced the high-speed stream, which followed and eventually compressed the ICME from behind. Overall, this analysis suggests how the solar wind context of CME-related events can be analyzed and understood using coronal and solar wind models.

Keywords: Heliosphere; Solar wind; Solar corona; Magnetic fields

1. Introduction

A general goal of space weather modeling efforts is the simulation of realistic events, including both the coronal mass ejection (CME) and its coronal and solar wind context. Toward this goal, it is reasonable to first investigate the simplest cases where the solar magnetic field is relatively simple and the event signatures are well defined. One such event that is particularly well documented and has been previously analyzed from multiple observational perspectives (e.g., Thompson et al., 1998; Webb et al., 2000) is the flare-related halo CME on May 12, 1997. Here we use this example to demonstrate how the application of a simple, magnetogram based coronal model can tell us about physical details of observed events not readily obtained by other means.

The May 12, 1997 halo CME occurred shortly after solar minimum when activity was low and the structure

*Corresponding author. Tel.: +1-937-255-3900.
E-mail address: nick.arge@noaa.gov (C.N. Arge).

1364-6826/$ - see front matter © 2004 Elsevier Ltd. All rights reserved.
doi:10.1016/j.jastp.2004.03.018

of the corona and solar wind was relatively simple. It was associated with the only active region on the solar disk (NOAA AR 8038), which was located north of the equator near central meridian. The active region was rapidly evolving, of new cycle polarity, and generated the only major flare of the day, which began at 04:42 UT and peaked around 04:55 UT. The flare was first visible in Hα and was associated with a filament that erupted soon thereafter followed by a pair of expanding Hα ribbons. The subsequent X-ray flare emission came from a small arcade that had formed over the region where the filament erupted. Twin dimming regions (positioned North-East and South-East) flanked the filament eruption. A classic EIT wave occurred during this event (Thompson et al., 1998).

The halo CME was observed in SOHO/LASCO C2 instrument at 06:30 UT with an estimated frontal speed of ~ 600 km/s (Plunkett et al., 1998) and onset time between 04:30-05:00 UT. Odstrcil et al. (2004) recently modeled this event using the numerical ENLIL solar wind model (Odstrcil and Pizzo, 1999a, b) and found that by assigning a speed of 650 km/s to the CME front at $24R_{\odot}$ (as determined by Zhao et al. (2002) using their cone model) they were able to achieve good agreement between the simulated and observed arrival time of the ICME at L1. For about 10 days before the event, the Earthward directed solar wind consisted of relatively slow (i.e., bulk flow speed less than 400 km/s) dense ambient material. The shock produced by the interplanetary coronal mass ejection (ICME) arrived at L1 early on the 15th followed by a magnetic cloud and then a high-speed stream, which is speculated (Webb et al., 2000) to have compressed the cloud from behind. The ICME produced a moderate geomagnetic storm with a maximum Dst of −115 nT. Fig. 1 summarizes the key solar wind plasma parameters from the WIND satellite for the nine-day period centered on the May 15th ICME arrival at L1, as well as the Dst geomagnetic index as provided by Kyoto University (http://swdcdb.kugi.kyoto-u.ac.jp/dstdir/). More comprehensive summaries of the event can be found in papers by Webb et al. (2000), Thompson et al. (1998), and Plunkett (1998) along with the references found therein.

In this paper we report on our efforts to model the ambient solar wind out to 1 AU around the time of the May 12, 1997 Halo CME and to identify its coronal source regions. We use the simple physics and empirical based Wang–Sheeley–Arge (WSA) model to do this. We

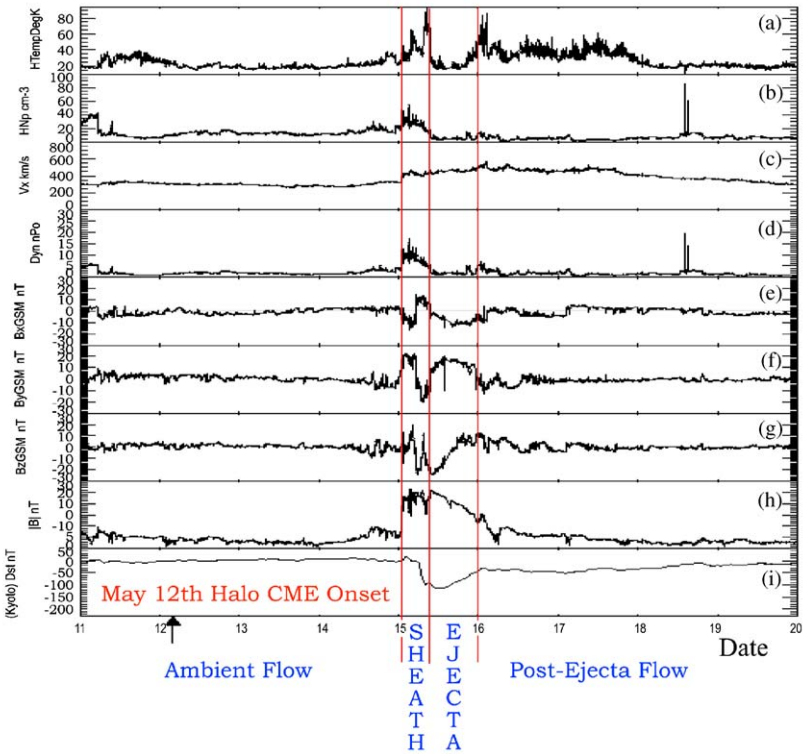

Fig. 1. Solar wind key plasma parameters from the WIND satellite (a–h) and the Dst geomagnetic index (i) as provided by Kyoto University (http://swdcdb.kugi.kyoto-u.ac.jp/dstdir/) for the nine-day period May 11–20, 1997. (a) Proton temperature (K), (b) Proton number density (cm^{-3}), (c) V_x ($km\,s^{-1}$) , (d) Dynamic Pressure (nPa), (e) $B_{x(GSM)}$ (nT), (f) $B_{y(GSM)}$ (nT), (g) $B_{z(GSM)}$ (nT), (h) $|B|$ (nT), (i) Dst (nT). The red vertical lines separate the different types of solar wind plasma labeled at the bottom of the plot.

find that the model describes the ambient solar wind stream structure around the time of the May 15, 1997 ICME generally well, except for the ejecta itself. The results presented here are consistent with those found independently by Odstrcil et al. (2004). In the next section, we provide a description of the WSA model and then briefly discuss the photospheric field data used as its input. In Section 3, we present and interpret the WSA modeling results. In Section 4, we discuss the implications of the suprathermal electron signatures as it pertains to the May 12th halo CME. We summarize our results in Section 5.

2. Empirical modeling of the event

2.1. The Wang–Sheeley–Arge model

The WSA model is a combined empirical and physics-based representation of the quasi-steady global solar wind flow. It can be used to predict the ambient solar wind speed and interplanetary magnetic field (IMF) polarity at Earth (as well as any other point in the heliosphere) and is thus useful for forecasting recurrent interplanetary disturbances. It is an improved version of the original Wang and Sheeley (WS) model (Wang et al., 1992). The model (original and improved) uses ground-based line-of-sight observations of the Sun's surface magnetic field as input to a magnetostatic potential field source surface (PFSS) model (Schatten et al., 1969; Altschuler and Newkirk, 1969) of the coronal expansion. The effects of outward flows in the corona, which are not explicitly contained in the formulation, are approximated by the imposition of radial boundary conditions at the so-called source surface, which is a Sun-centered sphere typically situated at 2.5 solar radii ($R_{\odot}$). In the original WS model, the interplanetary solar wind velocity is determined at each point on the source surface by the relative expansion of the magnetic field from the photospheric base up to that point, as provided by the model. This relation between expansion factor and wind speed is empirical and stems from correlation studies utilizing source surface expansion maps and near-Earth spacecraft observations of solar wind speed (Wang and Sheeley, 1990). In addition, the original WS model assumes that the solar wind flow propagates kinematically out from the source surface to Earth, with all dynamics neglected.

A number of important improvements have been made to the WS model (Arge and Pizzo, 1999, 2000; Arge et al., 2003) that has significantly improved its performance. These improvements can be divided into two categories: (1) improvements to the model input, which are the line-of-site (LOS) photospheric field measurements, and (2) improvements to the model itself.

The photospheric magnetic field is the sole quantitative large-scale physical observable, and a number of studies (Hoeksema et al., 1983; Zhao et al., 1997; Arge and Pizzo, 2000) have demonstrated that the details in assembling the raw individual magnetograms into a global, synoptic characterization are crucial for model accuracy. Depending on the data source used, a number of corrections may need to be applied to these data, which include accounting for LOS projection effects, line saturation effects, introduction of monopole moments, and polar field corrections. Other factors that must be addressed are data gaps and the quality of the data itself. In addition, frequent updating of the photospheric field maps with the latest magnetograms improves the WSA model predictions (Arge and Pizzo, 2000). The specific corrections applied to the photospheric field data used in this study are discussed in Section 2.2.

Three main improvements have been made to the original WS model. The first is the incorporation of a simple 1-D modified kinematic model (1-DMK), which includes an ad hoc method to account for stream interactions, to transport the wind from the outer boundary of the magnetostatic solution of the corona out to L1. (Simple 1-D kinematic solar wind propagation schemes similar to ours were first developed years ago (e.g., Hakamada and Akasofu, 1982)). The second is the use of Schatten current sheet (SCS) model (Schatten, 1971), which was added to provide a more realistic magnetic field topology of the upper corona region from 2.5 $R_{\odot}$ out to between 5.0 and 21.5 $R_{\odot}$, depending on which propagation model (e.g., the WSA 1-DMK model or an MHD model) is used to transport the solar wind out to 1 AU. We couple and solve the SCS and PFSS models using the same method as that of Wang and Sheeley (1995). The only difference in our approach is that we use the SCS solution out to a fixed radial distance that is still relatively close to the Sun (less than 0.1 AU), beyond which a propagation model is used to transport the solar wind out into the heliosphere. A more sophisticated current sheet model developed by Zhao and Hoeksema (1995), which is based upon the magnetostatic equilibria of Bogdan and Low (1986), is scheduled for testing in the WSA model in near the future.

The third modification made to the original WS model is the improvement to the empirical relationship relating coronal parameters to solar wind speed. The usual approach taken by Wang and Sheeley (1990, 1992) has been to divide magnetic field expansion factors (f_s) into finite number of bins, typically five, and then to assign a fixed solar wind speed to each range of f_s. Early on Arge and Pizzo (1999) developed a continuous empirical function relating magnetic field expansion factor and solar wind speed (v_{sw}) at 2.5 $R_{\odot}$ (i.e., at the source surface) rather than at L1, as traditionally done

by Wang and Sheeley (e.g., Wang and Sheeley, 1990, 1992). This empirical function was found by iteratively testing various mathematical relationships between f_s and v_{sw}, using it to assign the solar wind speed at the source surface, propagating the wind out to L1 using the 1-DMK model, and then comparing the results with observations. The procedure was repeated until a best fit was found. Before the inverse correlation between solar wind speed and magnetic field expansion factor was discovered by Wang and Sheeley (1990), Fry and Akasofu (1987) attempted (with modest success) to predict solar wind parameters using an empirical velocity equation that was a function of magnetic latitude.

Using daily updated synoptic maps from Mount Wilson Solar Observatory (MWO) and the PFSS + SCS model combination, Arge et al. (2003) recently found a new and improved empirical relationship for solar wind speed that is a function of two coronal parameters, f_s and the minimum angular separation (at the photosphere) between an open field footpoint and its nearest coronal hole boundary (θ_b). The second parameter, θ_b, has been routinely used by Riley et al. (2001) for a number of years now to empirically specify solar wind speed near the Sun. In effect, our relationship combines the methods of Wang et al. and Riley et al.. The new relationship works much better than the one we derived previously, which is a function of f_s only, in that it specifies solar wind speed at the boundaries and the interiors of coronal holes much more realistically. A recent (yet to be published) expanded comparison (spanning nearly an entire solar cycle) between predictions made using the old and new empirical relationships suggests that the new relationship in combination with setting the outer radius of the SCS model to 5.0 $R_\odot$ improves the WSA models' overall prediction performance. We are in the process of quantifying the improvement.

2.2. Model input

The photospheric field observations are the sole large scale observable and serve as a key driver to all coronal and solar wind models models. For this work, we used updated photospheric field synoptic maps (i.e., synoptic maps updated frequently with new magnetograms) constructed with line-of-sight (LOS) magnetograms from MWO and the MDI instrument on board the Solar Heliospheric Observer (SOHO) spacecraft. Since observational evidence suggests that the solar magnetic field is nearly radial at the photosphere, except in strong active regions (Harvey and Worden, 1998; Wang and Sheeley, 1992; Svalgaard et al., 1978), the LOS field measurements from these two data sources have been converted to radial. We now provide here a brief summary of the most pertinent facts about the updated synoptic maps used in this study. More details can be found in the references provided below.

2.2.1. MWO daily updated maps

An advantage to the maps from Mount Wilson Solar observatory is that they are updated with a large number (often more than 10) of magnetograms each day, depending on observing conditions, which reduces significantly the noise in the magnetic field measurements. As a comparison, only up to three magnetograms are taken each day at Wilcox solar observatory, and until SOLIS became operational in the Fall of 2003, only one magnetogram was typically taken each day at Kitt Peak solar observatory. Another advantage to the MWO data is that they have relatively few data gaps. A disadvantage to the MWO synoptic maps is that they require a number of corrections be applied to them before being used in the model. However, this is not a problem unique to data from MWO. For this study, we applied corrections to the MWO synoptic maps for line saturations effects and the polar fields. We now briefly explain and summarize these corrections.

Measurements of the LOS photospheric field at MWO are made using the Fe I 525.0 nm line. This line is known to be especially prone to line saturation effects (Ulrich, 1992; Ulrich et al., 2002), and field values derived from it must therefore be modified by an appropriate correction factor. By comparing photospheric field strengths derived from the Fe I 525.0 nm line to those derived from the Fe I 523.3 nm line Ulrich (1992) developed such a correction factor, and we have applied it to the set of daily updated MWO maps used in this study. Measurements of the LOS photospheric field near the Sun's poles are often highly unreliable because of their close proximity to the limb (i.e., only a small component of the field vector is directed toward the observer) and because the Sun's rotation axis is inclined 7.25° to the ecliptic plane. Regions located within 7.25° of the poles are in fact not even observable from Earth for up to six months at a time. In an effort to compensate for the problems associated with the LOS polar field measurements, Arge and Pizzo (2000) have developed a technique to both correct and fill (when necessary) the polar field measurements in synoptic maps. The main idea is to use polar field observations (1) during periods when they are well observed (i.e., when they are directed nearly at maximum toward the Earth) and (2) that span a time interval long before and after the period of interest. A polynomial curve is then fitted to these data and used to "correct" the polar field values in the synoptic maps of interest, such as all of the MWO maps used in this study.

2.2.2. Updated SOHO/MDI synoptic maps made with the Schrijver flux transport data assimilation model

Schrijver et al. (Schrijver, 2001; Schrijver and Title, 2001; Schrijver et al., 2002) have recently developed a new flux transport algorithm that can be updated regularly through the assimilation, by direct insertion,

of new magnetograms. The algorithm imports into a synoptic map the magnetic field data lying within 60° of the disk center of a new magnetogram and then evolves the field over the entire map, taking into account differential rotation, meridional flow, and supergranular diffusive dispersal. To maintain the quiet network outside the region, where the new field values have been assimilated, they inject small magnetic bipoles, a feature unique to their model (see Schrijver, 2001, for details). The photospheric fields residing at latitudes greater than |60°| are replenished and evolve over time strictly as a result of the transport algorithm. The evolution of the field continues until a new magnetogram is once again available, upon which it is assimilated into the map and the cycle repeated. Unlike the maps from MWO, Schrijver et al. has found no need to apply correction factors to the SOHO/MDI photospheric field values, except for the anomaly of multi-cycle simulations where they have found (Schrijver et al., 2002) it necessary to introduce an ad hoc decay time scale of 5 years for the field to improve the correspondence between data and observations. For short-term simulations, as in this study, this has no impact at all. A set of updated SOHO/MDI synoptic maps was generated using this algorithm for Carrington rotation (CR) 1922 (April 25–May 23, 1997), which encompasses the time of the May 12, 1997 CME. These maps were used in the WSA model to predict solar wind parameters at Earth and thus provide an independent check to the results obtained using the MWO maps.

3. Results

3.1. Qualitative comparison of the predicted and observed coronal holes

As a first step in our effort to understand the stream structure and coronal sources of the solar wind around the time of the May 12, 1997 CME, we compare the observed coronal hole structure for CR1922 with that predicted by the potential field source surface and Schatten current sheet (PFSS + SCS) model combination. Fig. 2a is the SOHO/EIT 284 Å synoptic map as constructed by E. Benevolenskaya (Benevolenskaya et al., 2001) at Stanford University (additional maps are available at http://quake.stanford.edu/~elena/EIT/). Fig. 2b shows the coronal holes as determined by the PFSS + SCS model combination. The solar wind speed values (at 5 $R_\odot$) also shown in Fig. 2b were derived empirically using the following relationship.

$$V(f_s,\theta_b) = 265.0 + \frac{1.5}{(1+f_s)^{1/3}}\{5.9 - 1.5e^{(1-(\theta_b/7.0)^{5/2})}\}^{7/2}\,\mathrm{km\,s^{-1}}, \quad (1)$$

where f_s is the flux tube expansion factor and θ_b the minimum angular separation (at the photosphere) between an open field footpoint and its nearest coronal hole boundary. We have placed the outlines of the predicted coronal holes, on top of Fig. 2a. As can be seen, the agreement between the predicted and observed coronal holes is, qualitatively, good. The regions of apparent discrepancy between the observed and predicted holes (e.g., the area in the northern polar region centered on longitude ~ 250° with an angular width of ~ 100°) are almost certainly due to bright, high altitude coronal structures lying in between the LOS of the observer and the coronal holes. The reality of the two small, isolated coronal holes (i.e., longitude ~ 130° and latitude ~ −30°; longitude ~ 200° and latitude ~ 30°), at lower latitudes is unclear. Unfortunately, the coronal hole contrast is low near solar minimum when the hot corona is largely absent.

3.2. Observed and predicted solar wind speed and IMF polarity at L1

In Fig. 3, the solar wind speed observations from the WIND satellite are compared with WSA predictions using the PFSS + SCS + 1-DMK model combination for a three Carrington rotation (CR) time interval (i.e., CR 1921–1923) that is roughly centered about the May 15, 1997 ICME. Not only does the plot provide one with a sense of how well the model reproduces the structure of the high-speed stream (the main focus of this paper) that followed the ICME, but also its performance over much longer time intervals before and after the event (approximately one and one-half Carrington rotations or ~ 40 days), as well as the model's general performance near the minimum phase of the solar cycle. The vertical bars seen in the figure are uncertainty estimates determined by finding the maximum and minimum values of the predicted solar wind speed at the sub-earth point as well as for those points located 2.5° above and below (i.e., north and south, respectively) them. They therefore provide an estimate of the range over which the solar wind speed can reasonably vary over a 5° latitude range, which is the resolution of the grid cell size (i.e., 5° × 5°) on the maps. The red dotted line is the base 10 logarithm of the plasma beta (β, ratio of thermal and magnetic pressures) parameter, which is calculated using the plasma data from the WIND satellite. Small plasma β values (i.e., $\log_{10}\beta$) $\leqslant -1.0$ often indicate the passage of transient solar wind where ambient solar wind models such as WSA are not expected to perform well. We use the plasma β parameter here to help with the identification of such transients. When available, we also use the O7+/O6+ ratio (Zurbuchen et al., 2002) for this purpose.

In Fig. 4, the solar wind IMF polarity observations from the WIND satellite are compared with WSA

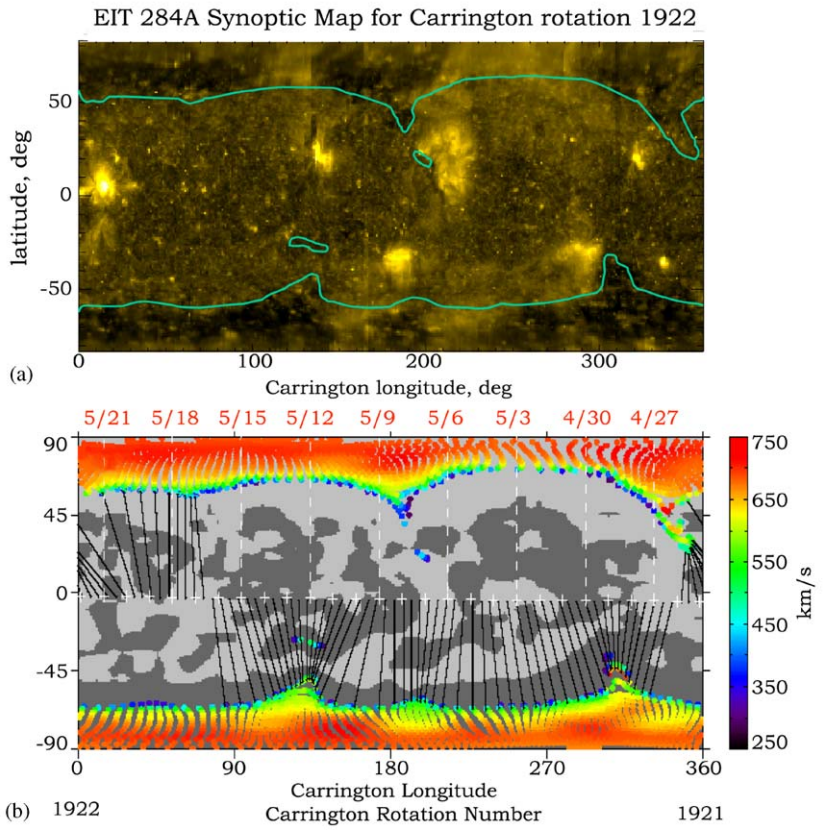

Fig. 2. (a) SOHO/EIT 284 Å synoptic map as constructed by Elena Benevolenskaya at Stanford University (http://quake.stanford.edu/~elena/EIT/). (b) Coronal holes as determined by the PFSS + SCS model combination. The field polarity at the photosphere is indicated by the light (positive polarity) and dark (negative polarity) gray contours, while the colored dots identify the footpoints of the open field lines (i.e., the coronal holes) at the photosphere. The dot color indicates the solar wind speed at 5.0 $R_{\odot}$ (see color bar scale to the right of the figure) as predicted by the model. The white plus signs near the equator mark the daily positions of the sub-earth point (the plus signs mark the beginning, i.e., 00:00 h, of each day indicated). The black straight lines identify the connectivity between the outer (open) boundary located at 5.0 $R_{\odot}$ and the source regions of the solar wind at the photosphere (1.0 $R_{\odot}$). On top of Fig. 2a, we have placed the outlines (i.e., green lines) of the coronal holes as predicted by PFSS + SCS model combination seen in Fig. 2b.

predictions for the same time interval as for the solar wind speed comparisons in Fig. 3. The open blue triangles correspond to IMF polarity predictions for those points located 2.5° in latitude above and below the sub-earth points. They are analogous to the vertical bars in the solar wind speed plots. When different polarity values are obtained for a given date and time, then the sub-earth point is located very near the current sheet. The sky-blue dashed line in the plots is the value of the solar b angle. During CR1921 and to a lesser degree CR1922, the solar b angle was large and negative implying that the north pole of the Sun was poorly observed from the Earth.

On the whole, WSA captures the large-scale, ambient stream structure over the three Carrington rotation time intervals reasonably well. The results displayed were obtained using daily updated maps. There are, however, some noticeable discrepancies between the predictions and observations, most of which are likely explained by the occurrence of transient events and the flatness of the current sheet (which is typical during this stage of the solar cycle). For instance, a well-known CME occurred on April 7, 1997 (see Webb et al., 2000 and references therein) with the ensuing ICME arriving four days later on April 11. The plasma β is extremely small for a fraction of a day on April 11, which helps confirm the arrival and subsequent passage of transient material. The flatness of the current sheet during solar cycle minimum makes predicting solar wind stream structure especially difficult. Since the transition from slow to fast wind (or vice versa) can be quiet rapid, a small uncertainty in the predicted position of the current sheet, depending on its orientation, can result in significant model error. When the current sheet is highly

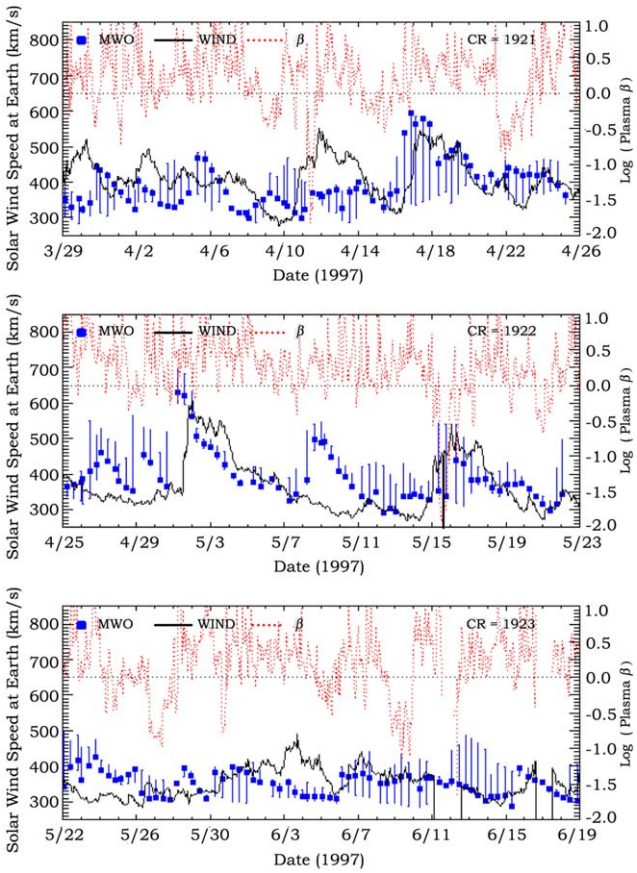

Fig. 3. Comparison of solar wind speed observations (thin black solid line) from the WIND satellite with WSA predictions (small blue squares) for CR 1921–1923. The vertical bars are uncertainty estimates determined by finding the maximum and minimum values of the predicted solar wind speed at the sub-earth point as well as for those points located 2.5° above and below them. The red dotted line is the base 10 logarithm of the plasma beta (β, ratio of thermal and magnetic pressures) parameter determined using the WIND satellite plasma data.

warped, the sub-earth point cuts across the current sheet in a more perpendicular fashion, as the Sun rotates, instead of more parallel/tangential to it, as when it is nearly flat. A small shift in latitude of the current sheet (perhaps resulting from incorrect polar fields values) would thus most likely have minimal effect on the predictions during solar maximum but potentially introduce significant errors during solar minimum. For instance, the discrepancies between observations and predictions during the three-day period May 8–11, 1997 may be a result of the flatness of the current sheet, since the sub-earth point was frequently located very close to it (in the daily updated synoptic maps used to make those predictions). Using higher resolution maps may help to reduce some of these problems.

Finally, we have noticed a pattern with the WSA model where significant discrepancies occur between model predictions and observations, for periods up to 2–3 days after the passage of transient wind, when the (observed) solar wind has returned back to ambient conditions and where the model is expected to resume performing well. This pattern is not unique to just CR1921-1923 but appears in comparisons spanning nearly an entire solar cycle. The stream following the April 11 ICME is one example of this. One possible explanation for this is a change in the coronal configuration after the occurrence of a transient. Since photospheric field synoptic maps are not instantaneous snapshots of the Sun's field but rather an assembly of 27-days of magnetograms that are, usually, merged together using a weighting function sharply peaked at central meridian, sudden and/or subtle changes in the photospheric field configuration are likely often masked in these maps, especially those assembled in the manner just described. Therefore, sudden and/or subtle changes in the coronal hole configuration (e.g., after transients)

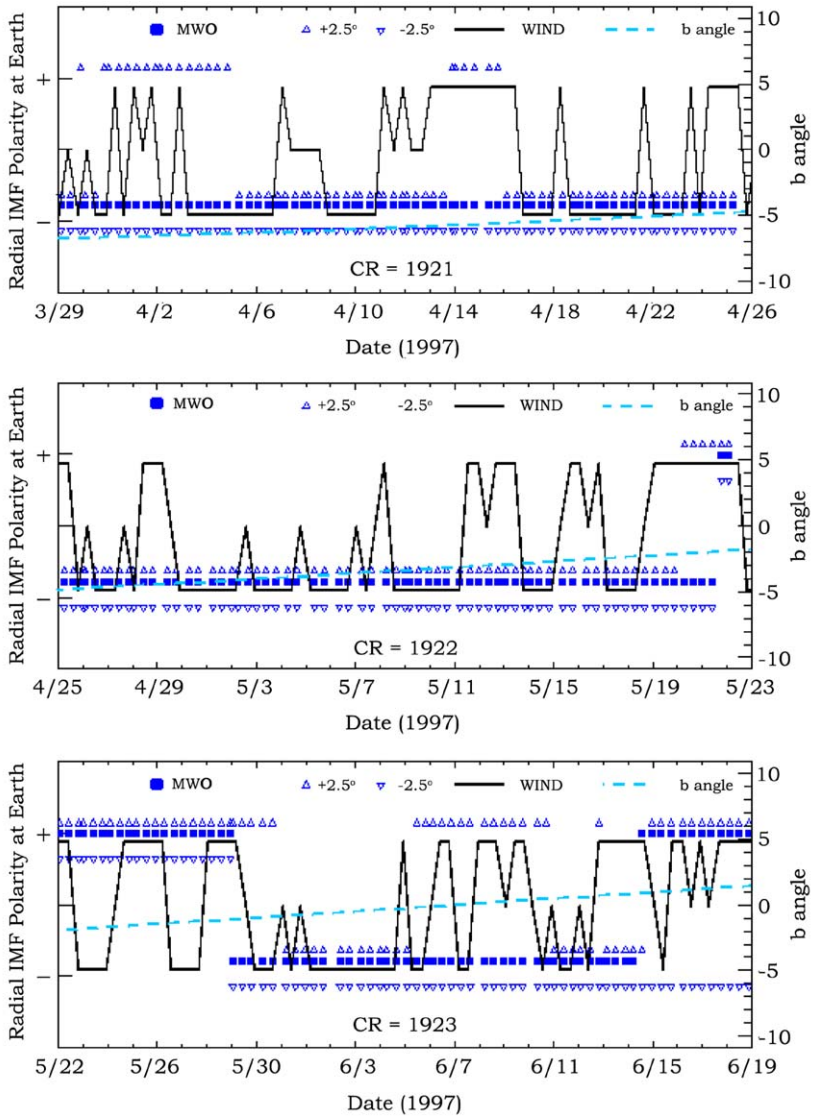

Fig. 4. Solar wind IMF polarity observations (thin solid back line) from the WIND satellite are compared with WSA predictions (small blue squares) for CR 1921–1923. The open blue triangles correspond to IMF polarity predictions for those points located 2.5° in latitude above (upward pointing triangles) and below (downward point triangles) the sub-earth points. They are analogous to the vertical bars in the solar wind speed plots. The sky blue dashed line in the plots is the value of the solar *b* angle (latitude of Earth in solar equatorial system).

are, by implication, possibly missed (perhaps frequently) in the models. In spite of these difficulties related to flat current sheets and transients, one can see that several major high-speed streams in Fig. 3 (e.g. April 16–22, May 1–7) are captured with the model. The important stream from the viewpoint of the present study is on May 12–19. The results for this period in Fig. 3 are consistent with the overall observations of a medium-speed stream with peak velocities of $\sim 450\,\mathrm{km/s}$. The May 15 ICME resides at the leading edge of the stream during the low beta time interval.

3.3. Coronal sources

Displayed on the right-hand-side of Fig. 5 are the global coronal field polarity at 5 $R_\odot$, the solar wind speed at 5 $R_\odot$ (as determined by Eq. (1)), and the open field (or coronal hole) configuration at the photosphere

(similar to the map in Fig. 2a), all of which were derived using the combined PFSS + SCS model and the photospheric field synoptic map, last updated with a new magnetogram at approximately the beginning of May 14, 1997. This particular map was selected for display as it shows the source region of the stream that followed and compressed the May 12th CME from behind after it is fully developed and most evident in the maps. In the coronal polarity plot (Fig. 5c) white (black) denotes magnetic field directed outward (inward), from the Sun, corresponding to positive (negative) polarity in the IMF polarity plots shown in Fig. 4 and in the lower left corner of this figure. As mentioned earlier, the current sheet is rather flat for CR1922 and the sub-earth points (red plus signs) often lay close to it.

On the left-hand-side of Fig. 5 are plotted the WSA solar wind speed and IMF polarity predictions versus WIND satellite observations for CR1922. The light green shaded areas in the two plots correspond to the time-interval of the ICME passage (sheath plus ejecta) as discussed and shown in more detail in Fig. 1. Here, as expected, the WSA model fails to capture the transient stream properties. However, the model reproduces, within reason, the observed solar wind speed profile

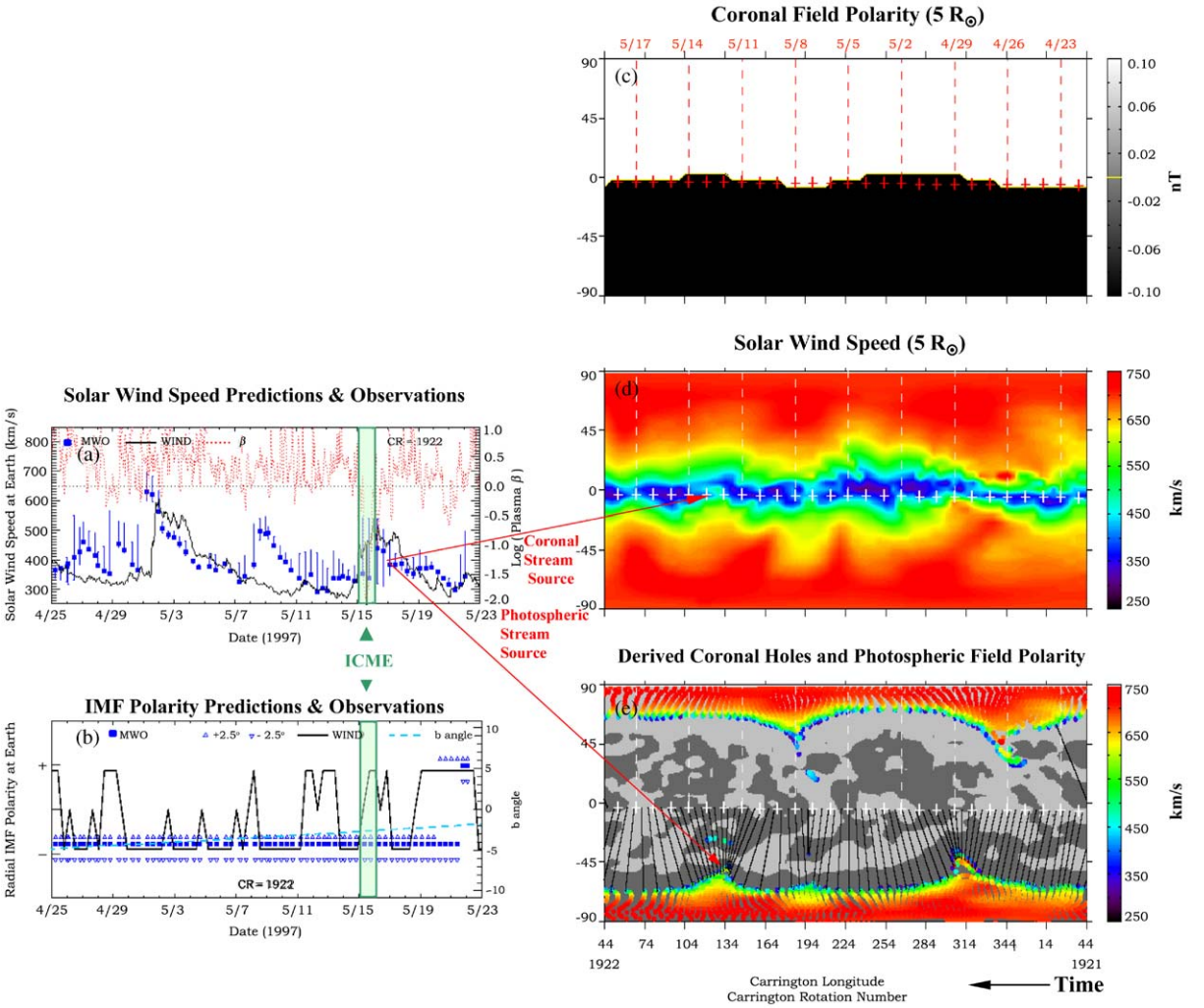

Fig. 5. On the right-hand side: (c) the global coronal field polarity at 5 $R_{\odot}$, (d) the solar wind speed at 5 $R_{\odot}$, and (e) the open field (or coronal hole) configuration at the photosphere (similar to the map in Fig. 2a), all of which were derived using the combined PFSS + SCS model and the photospheric field synoptic map last updated with a new magnetogram at approximately the beginning of May 14, 1997. Left-hand side: WSA solar wind speed (a) and IMF polarity (b) predictions versus WIND satellite observations for CR1922. The light green shaded areas in the two plots correspond to the time-interval of the ICME passage (sheath plus ejecta). The red arrows identify the stream sources at 5 $R_{\odot}$ and 1$R_{\odot}$. Note that time runs from right to left in synoptic maps.

for a number days before and after the passage of the ICME, and the IMF polarity is correctly predicted for at least a day before and after (i.e., following the day of fluctuating polarity beginning on 16th) the ICME. In Fig. 5d, the modest high-speed region (i.e., light green area) lying in between the two sub-earth points corresponding to the 12th and 13th of May is the source (at 5.0 $R_{\odot}$) of the earth-directed stream that followed the transient. As can be seen in the figure, the peak flow speed in this region occurs around mid-day on the 12th after the CME launch, which happened earlier in the day. The coronal source of this modest high-speed stream is the coronal hole extension located in the southern hemisphere (Fig. 5e) at $\sim 130^{\circ}$ longitude. We followed the evolution of this coronal extension going back to the beginning of May 8th using PFSS + SCS model driven by daily updated photospheric field maps. We found that the coronal hole broadened longitudinally with time and began extending further northward, from its original northern most extent of about -55° latitude on the 8th, reaching up to about -45° latitude around the time of the CME eruption on the 12th. Not until late on the 11th did the modest high-speed region (i.e., light green area visible in Fig. 5d), begin to appear between the May 12th and 13th sub-earth points. The above discussion identifying the coronal source of the high speed-stream along with the coronal polarity map shown in Fig. 5c makes it clear why the IMF predictions are in agreement with observations only roughly a day before and after the ICME event. As seen in the figure, the sub-earth point clearly lies south of the current sheet, where the IMF polarity is negative, from about mid-day on the 11th until early on the 14th. However, before and after this time, the sub-earth points lie very near the current sheet, where predictions of the IMF are often highly uncertain (note the mixed polarity predictions on ~May 20th in Fig. 5b).

In Fig. 6, we display the same WSA predictions for CR1922 but now with the model driven by Schrijver et al.'s SOHO/MDI updated synoptic maps. Not only do these results support the conclusions arrived at using the MWO maps, but they are in better overall agreement with the observations, especially for the IMF. The over prediction in speed that occurred from May 8–11, 1997 in the MWO results, (i.e., Fig. 3) is still there, but is not as pronounced. In addition, the largest over estimates in speed (occurring on May 8) have uncertainty bars that are large and encompass, save one, the observed solar wind speed unlike those for MWO. The predictions from May 25–30 are missing in the plot, because we ran the Schrijver photospheric field maps using data only from CR1922. Since the solar wind takes on average 4–5 days to reach Earth, the predictions based on the data from the beginning of CR1922 (April 25, 1997) arrived $\sim$ 5 days later on the 30th. Schrijver et al. updates their maps four times a day and this explains

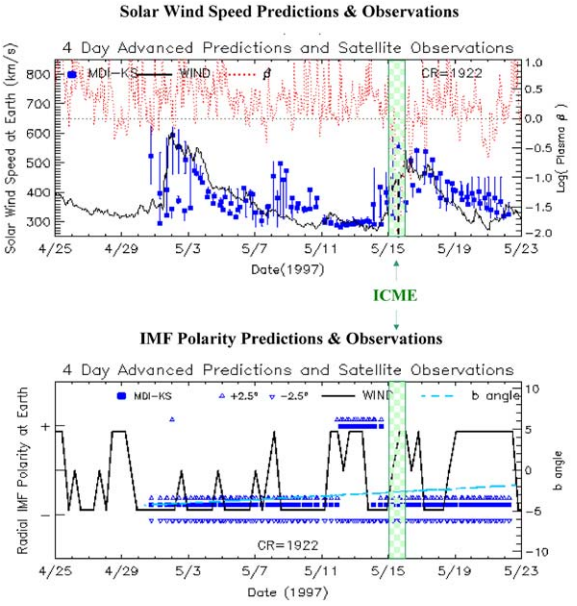

Fig. 6. WSA solar wind speed and IMF polarity predictions at Earth and WIND satellite observations for CR1922 using the Schrijver et al.'s updated SOHO/MDI synoptic maps as input.

the larger number of predictions per day compared to those from MWO.

3.4. Role northern active region played in the stream following ICME

The results presented above suggest that the stream that followed the May 15th ICME came from a coronal hole located in the southern hemispheric, while the May 12th CME itself is known to be associated with the only active region on the solar disk (NOAA AR 8038), which was located north of the equator near central meridian. In an effort to determine what, if any, role the northern active region played in the generation of the modest high-speed stream that followed the ICME, we removed the northern active region from a subset of the daily updated photospheric field maps used in this study corresponding to a few days before and after the May 12th CME. For each map, we manually removed the active region and then replaced it with the nearby weak field values. On the left-hand-side of Fig. 7, at the top, is the daily updated photospheric field synoptic map last updated with a new magnetogram on the May 12th. At top right in the figure is the same map but now with the northern active region removed. Using these modified maps in the WSA model, new solar wind predictions were generated. The solar wind speed and IMF polarity predictions with and without the active region are also plotted in Fig. 7. As can be seen, there is virtually no difference in the two sets of predictions, although the

IMF polarity results are in better agreement with the observations after May 21st for the maps with the active region removed. These results, along with the fact that the stream source appeared on the solar wind speed maps (see discussion in Section 3.3) on the 11th, i.e., before the CME launch, suggest that neither the northern active region nor the CME played a role in producing the stream that followed the ICME. However, it is possible that whatever changes led to the development of the modest high-speed stream source also eventually caused the CME eruption. These results also explain why the model captured the stream after the passage of the ICME, when as mentioned earlier, the WSA model often fails for 2–3 days following

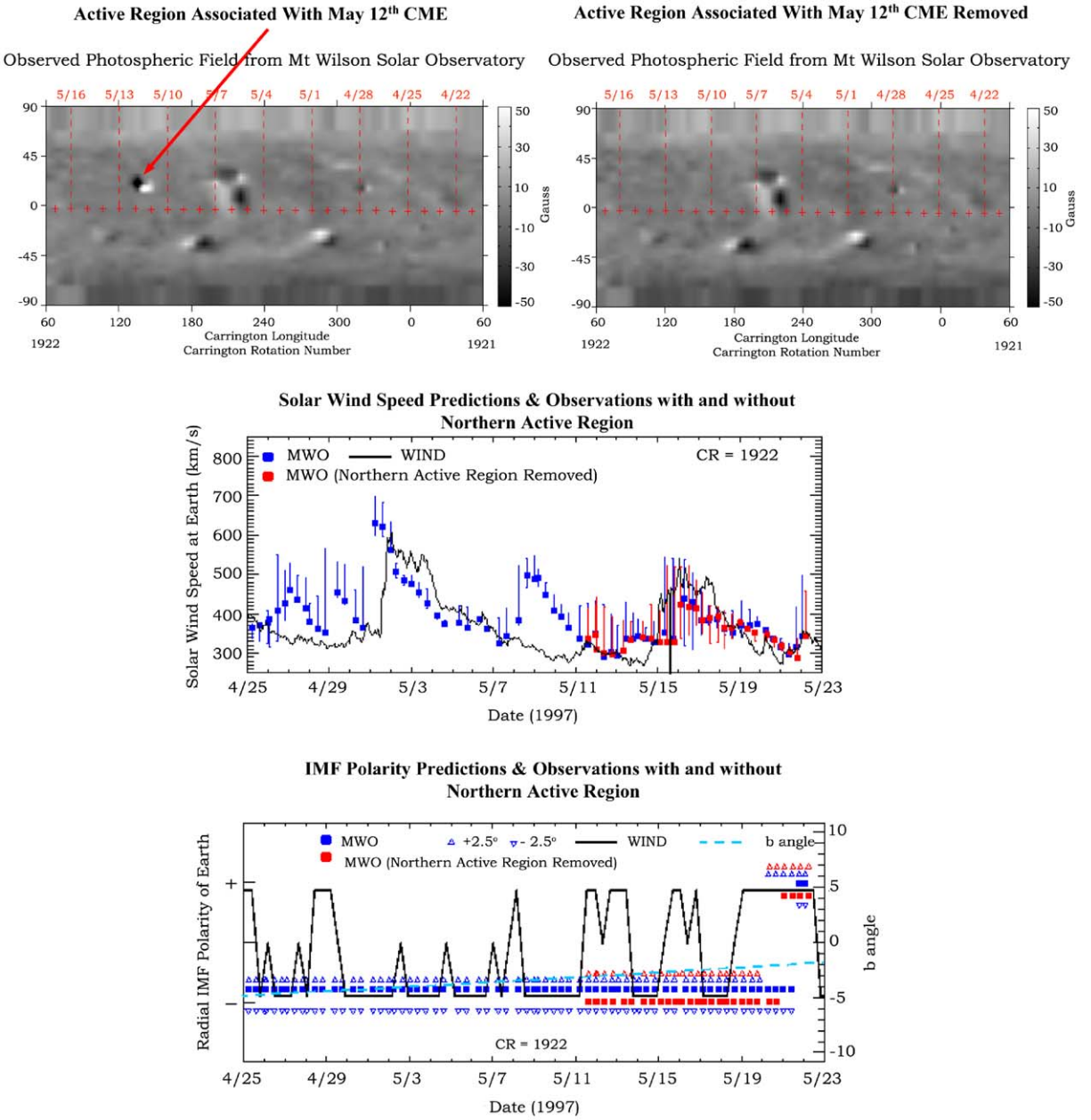

Fig. 7. (Top) Left hand side: Example of a MWO daily updated photospheric field synoptic map used in this study. (Top) Right hand side: Same as figure on the left but now with the northern active region removed. (Center) Solar wind speed and (Bottom) IMF polarity predictions when using MWO daily updated photospheric field maps with (small blue squares) and without (small red squares) the active region.

the passage of such a transient event—the CME did not play a role in the formation of the stream, since it developed first.

4. Implications of the suprathermal electron signatures

Fig. 8 shows a close-up of the in situ plasma and field behavior detected on the WIND spacecraft upstream of Earth during the period of the May 12, 1997 solar event-generated ICME. As noted elsewhere in this paper, this ICME occurs on May 15, at the leading edge of a modestly high-speed stream with roughly 500 km/s velocities. A preceding shock is clearly seen in the dynamic pressure, velocity, and magnetic field magnitude as a sharp increases. The following sheath portion of the ICME, composed of compressed ambient solar wind, contains a narrow current sheet, which could be the swept-up heliospheric current sheet. The subsequent combined density decrease and smooth, rotating enhanced magnetic field suggest that the ejecta, or driver signature of the ICME, arrives at WIND at about 10:00 UT on May 15 and lasts until at least 00:00 UT on May 16. Of special interest here is the information contained in the suprathermal electron anisotropies shown by the three color-coded pitch angle spectrograms.

Suprathermal solar wind electrons in the energy range from several hundred to ~ 1 keV are traditionally used as diagnostics of magnetic field topology, in particular of field connectivity to the Sun. These heat flux electrons typically have narrowly focused field-aligned angular distributions indicating streaming along open interplanetary magnetic field lines away from the Sun in the undisturbed solar wind. They are also known to exhibit periods of counterstreaming, indicating mirroring or field connections to the Sun at both ends, during intervals within ICME ejecta and sometimes in ICME sheaths (e.g., Gosling et al., 1987; Shodhan et al., 2000).

In this case it appears from the B_x and B_y components of the magnetic field that an interplanetary sector boundary crossing (from positive B_x and negative B_y to negative B_x and positive B_y) occurs just prior to or at the shock arrival time. The expected change in the electron streaming pitch angle from its initial 180° value antiparallel to the prevailing field (B_x positive, or toward the Sun in the standard GSE coordinates used), to 0°, or parallel to the field, is not seen at the time due to the proximity to the shock crossing. Instead, counterstreaming distributions are seen in the foreshock typical of reflected heat flux electron signatures also found upstream of the Earth's bow shock. The electron distribution is isotropized in the vicinity of the shock itself, probably due to the presence of enhanced wave-particle interactions or Coulomb scattering. In the sheath, the new 0° pitch angle streaming conditions presumably imposed just prior to the shock passage resume. There are several rotations in the North–South (z) component of the compressed magnetic field in the sheath, including the sharp current sheet crossing at about 06:00 UT on May 15. Interestingly, the heat flux electron anisotropy does not reverse at this time to its original upstream 180° pitch angle. Such signatures are referred to as false polarity reversals (e.g., Kahler and Lin, 1995) and are interpreted as bends or folds in the local field lines. The onset of significant fluctuations in the inclination of the field, seen in the B_z component about an hour earlier, may signify an encounter with structures in the sheath prior to entry into the ejecta proper. The heat flux anisotropy does reverse about two hours after the sharp current sheet passage, coincident with one of the rotations of the B_z component from southward to northward. At a second sharp current sheet crossing at about 10:00 UT on May 15, the ejecta signatures of lower plasma density and a smooth rotation in the magnetic field begin simultaneous with a last heat flux anisotropy reversal.

Notably, significant counterstreaming is nowhere evident within the provisional period of ejecta passage through 00:00 UT on May 16. Instead, the ejecta fields are inferred to be connected to the Sun at one end, consistent with an interplanetary field polarity opposite to that at the start of the plotted interval. Following the return to what seem to be ambient interplanetary conditions, the electron fluxes are lower, with anisotropies favoring the ejecta polarity signature but showing significant fluctuations and periods of possible weak counterstreaming. The anisotropies return to a strong 180° pitch angle signature, consistent with the pre-ICME southern hemisphere solar wind source, at about 04:00 UT on May 17.

The implication of these anisotropies is that the swept-up solar wind in the sheath contains the heliospheric current sheet crossing in addition to other field rotations of unknown origin. The ejecta portion consists of open field lines rooted at the Sun in a region with magnetic polarity opposite to that prior to arrival of the ICME shock. This interpretation would be consistent with the idea, inferred from the WSA model analysis described above, that the ambient solar wind coming from a southern hemisphere coronal hole extension is intruded upon by flows from the opposite polarity northern hemisphere containing the CME-associated flaring active region. The observed ejecta fields may have either become disconnected from the Sun at one end if they were originally closed loops, or WIND may have in fact missed the closed field portion of the ejecta and instead sampled a surrounding portion of northern hemisphere open field deflected southward during the event passage. This analysis illustrates that event contextual modeling together with suprathermal electron signature observations can be used to reinforce

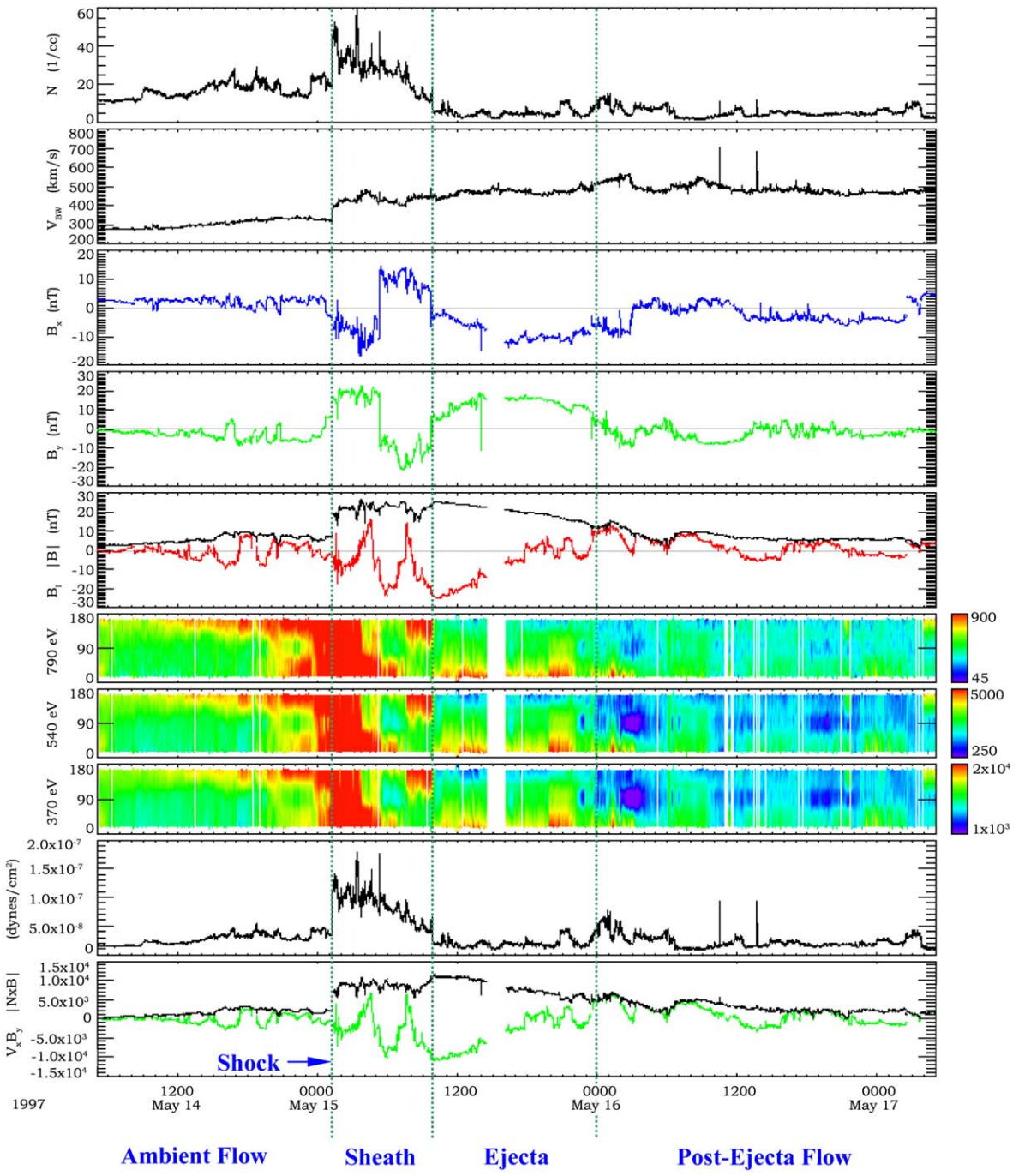

Fig. 8. Observations from the 3DP plasma spectrometers and the magnetometer on the WIND spacecraft during the passage of the ICME spawned by the May 12, 1997 CME. The panels show, from the top: plasma density, bulk velocity, magnetic field components and total field magnitude (components in the standard GSE coordinate system, with $+x$ pointing toward the Sun, and $+y$ and $+z$ pointing opposite the direction of planetary motion and northward, respectively), color spectrograms for three different energy electron fluxes (color indicates particles per square cm per second), plasma dynamic pressure (mass density times velocity squared), and northward and total convection electric fields $E = -V \times B$.

or negate envisioned CME ejection and propagation scenarios.

5. Summary and conclusions

We have modeled the ambient solar wind during the time of the May 12, 1997 CME using the Wang–Sheeley–Arge (WSA) model driven by two independent sets of photospheric field synoptic maps: daily updated maps from Mount Wilson Solar Observatory and updated SOHO/MDI maps constructed with the Schrijver et al. (Schrijver, 2001) flux transport data assimilation routine. We find that the WSA model can replicate the solar wind speed and IMF polarity profiles for this time-period rather well except for the ejecta itself, which is beyond the model's capability. The results presented in this paper as well as those of Odstrcil et al. (2004) both suggest that the source of the high-speed stream that followed and compressed the ICME from behind originated from a small coronal hole extension located south of the Sun's equator (see the Odstrcil paper for a 3-D view of the solar wind structure around the time of this event). Finally, the active region in the northern hemisphere associated with the May 12th CME does not appear to have played a role in either the formation or the general nature of the small southern coronal hole extension that produced the high-speed stream.

Our case study analyses more generally illustrate how one can use a magnetogram-based coronal/solar wind model to infer the origin(s) of the stream structure surrounding an ICME. Odstrcil and Pizzo (1999a, 1999b) experimented with MHD models of simplified simulated coronal ejections expelled into a solar wind produced by a high polar/low equatorial speed source organized around a planar tilted heliospheric current sheet. Their experiments with ejections above, below, and inside of the slow wind belt produce modeled time series at 1 AU showing how the ejecta fall within the evolved stream structure. On occasions where the ejection is in or above the slow speed belt in such a way that it is followed at the same latitude at a later time by the higher speed wind, the ejecta appear at the leading edge of a high-speed stream - much the same as the May 15, 1997 ICME observations in Fig. 1. However, the numerical experiments on a hypothetical simple scenario lacked the smaller-scale important coronal hole extensions present in the WSA model. The ecliptic solar wind near solar activity minimum can be highly influenced by relatively minor-looking coronal hole sources, such as the southern hemisphere coronal hole extension in our case study. In this case the ejecta coming from the source associated with the northern hemisphere flaring active region may have been pushed from behind by the stream from the southern hemisphere coronal hole extension. Thus it is important in models seeking to simulate and explain real events to have a sufficiently accurate description of the ambient corona and solar wind including detailed structures. While each CME and ICME will have their own nuances of coronal and solar wind context, our example illustrates the usefulness of routinely carrying out ambient state solar wind calculations for real CME event studies to help distinguish ambient corona from coronal dynamics effects. The WSA model represents one relatively low-computational-power way to carry out such analyses.

Acknowledgements

We would like to thank D. Larson and the WIND 3DP and magnetometer PIs R. Lin and R. Lepping for enabling our access to the WIND data. We thank R. Ulrich and the staff at Mount Wilson solar observatory for providing us routine access to their data and for being so accommodating with our particular data needs and requests. Leslie Mayer provided a significant amount of programming support for this project, and we sincerely thank her for all her diligent efforts. We also would like to acknowledge beneficial discussions related to this work at the annual SHINE conferences. This work is supported in part by the CISM project, which is funded by the STC Program of the National Science Foundation under Agreement Number ATM-0120950, and by grants NSF ATM-0001851, ONR No. 03PR06657-00, and AFOSR-ISSA-03-NM-062.

References

Altschuler, M.A., Newkirk Jr., G., 1969. Magnetic fields and the structure of the solar corona. Solar Physics 9, 131–149.

Arge, C.N., Pizzo, V.J., 1999. Historical verification of the Wang–Sheeley model: further improvements in basic technique. In: The Ninth International Solar Wind Conference. AIP, Melville, NY, pp. 569–572.

Arge, C.N., Pizzo, V.J., 2000. Improvement in the prediction of solar wind conditions using near-real time solar magnetic field updates. Journal of Geophysical Researach 105, 10465–10479.

Arge, C.N., Odstrcil, D., Pizzo, V.J., Mayer, L.R., 2003. Improved method for specifying solar wind speed near the sun. In: The Tenth International Solar Wind Conference. AIP, Melville, NY, pp. 190–193.

Benevolenskaya, E.E., Kosovichiev, A.G., Scherrer, P.H., 2001. Detection of high-latitude waves of solar coronal activity in extreme-ultraviolet data from the Solar and Heliospheric Observatory EUV Imaging Telescope. Astrophysical Journal 554, L107.

Bogdan, T.J., Low, B.C., 1986. The three-dimensional structure of magnetic atmospheres, II, modeling the large-scale corona. Astrophysics Journal 306, 271.

Fry, C.D., Akasofu, S.-I., 1987. Latitudinal dependence of solar wind speed. Planetary and Space Science 7, 913.

Gosling, J.T., Baker, D.N., Bame, S.J., Feldman, W.C., Zwickl, R.D., 1987. Bidirectional solar wind electron heat flux events. Journal of Geophysics Research 92, 8519.

Hakamada, K., Akasofu, S.-I., 1982. Simulation of three-dimensional solar wind disturbances and resulting geomagnetic storms. Space Science Reviews 31, 3–70.

Harvey, J., Worden, J., 1998. New types and uses of synoptic maps. In: Balasubramaniam, K.S., Harvey, J.W., Rabin, D.M. (Eds.), Solar Synoptic Physics (Astronomical Society of the Pacific Conference Series 140). ASP, Provo, UT, pp. 155–160.

Hoeksema, J.T., Wilcox, J.M., Scherrer, P.H., 1983. The structure of the heliospheric current sheet—1978–1982. Journal of Geophysicial Research 88, 9910.

Kahler, S., Lin, R.P., 1995. An examination of directional discontinuities and magnetic polarity changes around interplanetary sector boundaries using $E>2$ keV electrons. Solar Physics 161, 183.

Odstrcil, D., Pizzo, V.J., 1999a. Three-dimensional propagation of CMEs in a structured solar wind: 1, CME launch within the streamer belt. Journal of Geophysical Research 104, 483–492.

Odstrcil, D., Pizzo, V.J., 1999b. Three-dimensional propagation of CMEs in a structured solar wind: 2, CME launch adjacent to the streamer belt. Journal of Geophysical Research 104, 493–503.

Odstrcil, D., Riley, P., Zhao, X.P., 2004. Numerical simulation of the May 12, 1997 interplanetary CME event. Journal of Geophysical Research 109, doi:10.1029/2003JA010135.

Plunkett, S.P., Thompson, B.J., Howard, R.A., Michels, D.J., St. Cyr, O.C., Tappin, S.J., Schwenn, R., Lamy, P.L., 1998. LASCO observations of an Earth- directed coronal mass ejection on May 12, 1997. Geophysical Research Letters 25, 2477.

Riley, P., Linker, J., Mikic, Z., Lionello, R., 2001. MHD modeling of the solar corona and inner heliosphere: comparison with observations. In: Song, P., Singer, H., Siscoe, G. (Eds.), Space Weather (Geophysical Monograph Series 125). AGU, Washington D.C., p. 159.

Schatten, K.H., 1971. Current sheet magnetic model for the solar corona. Cosmic Electrodynanics 2, 232–245.

Schatten, K.H., Wilcox, J.M., Ness, N.F., 1969. A model of interplanetary and coronal magnetic fields. Solar Physics 9, 442–455.

Schrijver, C.J., 2001. Simulations of the photospheric magnetic activity and outer atmospheric radiative losses of cool stars based on the characteristics of the solar magnetic field. Astrophysical Journal 547, 475–490.

Schrijver, C.J., Title, A.M., 2001. On the formation of polar spots in Sun-like stars. Astrophysical Journal 551, 1099–1106.

Schrijver, C.J., DeRosa, M.L., Title, A.M., 2002. What is missing from our understanding of long-term solar and heliospheric activity? Astrophysical Journal 577, 1006–1012.

Shodhan, S., Crooker, N.U., Fitzenreiter, R.J., Larson, D.E., Lepping, R.J., Kahler, S.W., Gosling, J.T., 2000. Counter-streaming electrons in magnetic clouds. Journal Geophysical Research 105, 27261.

Svalgaard, L., Duvall Jr., T.L., Scherrer, P.H., 1978. The strength of the Sun's polar fields. Solar Physics 58, 225–239.

Thompson, B.J., Plunkett, S.P., Gurman, J.B., Newmark, J.S., St. Cyr, O.C., Michels, D.J., 1998. SOHO/EIT observations of an Earth-directed coronal mass ejection on May 12, 1997. Geophysical Research Letters 25, 2465.

Ulrich, R.K., 1992. Analysis of magnetic fluxtubes on the solar surface from observations at Mt. Wilson of λ 5250 and λ 5233. In: Giampapa, M.S., Bookbinder, J.A. (Eds.), Cool Stars, Stellar Systems, and the Sun. Astronomical Society of the Pacific, San Francisco, pp. 265–267.

Ulrich, R.K., Evans, S., Boyden, J.E., Webster, L., 2002. Mount Wilson synoptic magnetic fields: improved instrumentation, calibration, and analysis applied to the 2000 July 14 flare and to the evolution of the dipole field. Astrophysical Jounral Suppl. 139, 259–279.

Wang, Y.M., Sheeley, N.R., 1990. Solar wind speed and coronal flux-tube expansion. Astrophysical Journal 355, 726–732.

Wang, Y.-M., Sheeley Jr., N.R., 1992. On potential field models of the solar corona. Astrophysical Journal 392, 310.

Wang, Y.-M., Sheeley Jr., N.R., 1995. Solar implications of ULYSSES interplanetary field measurements. Astrophysical Journal 447, L143–L146.

Webb, D.F., Lepping, R.P., Burlaga, L.F., DeForest, C.E., Larson, D.E., Martin, S.F., Plunkett, S.P., Rust, D.M., 2000. The origin and development of the May 1997 magnetic cloud. Journal of Geophysical Research 105, 27251.

Zhao, X.P., Hoeksema, J.T., 1995. Prediction of the interplanetary magnetic field strength. Journal of Geophysical Research 100, 19.

Zhao, X.P., Hoeksema, J.T., Scherrer, P.H., 1997. Modeling boot-shaped coronal holes using SOHO-MDI magnetic measurements. Proceedings of the Fifth SOHO Workshop. Eur. Space Agency Spec. Publ., ESA SP-404, 751, 1997.

Zhao, X.P., Plunkett, S.P., Liu, W., 2002. Determination of geometrical and kinematical properties of halo coronal mass ejections using the cone model. Journal of Geophysical Research 107 (A8), SSH 13–1.

Zurbuchen, T.H., Fisk, L.A., Gloeckler, G., vonSteiger, R., 2002. The solar wind composition throughout the solar cycle: A continuum of dynamic states. Geophysical Research Letters 29, 1.